Research Square

Preprints are preliminary reports that have not undergone peer review.
They should not be considered conclusive, used to inform clinical practice,
or referenced by the media as validated information.

ACOT11 suppresses prostate cancer progression by inhibiting mitochondrial homeostasis and the PI3K/AKT signaling pathway

Yang Cui

892870669@qq.com

Shijiazhuang People's Hospital

Jin Zhao

Hebei General Hospital

He ran Cao

Shijiazhuang People's Hospital

Wei Li

Second Hospital of Hebei Medical University

Article

Keywords: acyl CoA thioesterase 11, prostate cancer, tumor suppressor, mitochondrial homeostasis, PI3K/AKT signaling pathway, proliferation

Posted Date: October 30th, 2026

DOI: https://doi.org/10.21203/rs.3.rs-10169833/v1

License: This work is licensed under a Creative Commons Attribution 4.0 International License.
Read Full License

Additional Declarations: No competing interests reported.

Abstract

Prostate cancer (PCa), a major malignancy in aged males, often advances to castration-resistant prostate cancer (CRPC) within two years with unclear mechanisms. Acyl CoA thioesterase 11 (ACOT11) modulates lipid metabolism and mitochondria, yet its function in PCa remains unclarified. This study investigated ACOT11's expression, role and mechanism in PCa. RT-qPCR and western blot tested ACOT11 levels in 20 PCa and 20 benign prostatic hyperplasia tissues. siRNA and overexpression plasmids modified ACOT11 in PC3 and DU145 cells; CCK-8, wound healing and Transwell assays assessed cell proliferation, migration and invasion. Flow cytometry, kits and transmission electron microscopy detected mitochondrial function and ultrastructure. Western blot examined PI3K/AKT, mitochondrial and autophagy proteins. ACOT11 was markedly low in PCa samples. ACOT11 silencing boosted PC3 cell malignant phenotypes, while its overexpression suppressed DU145 progression, triggering mitochondrial dysfunction, repressing PI3K/AKT phosphorylation, modulating MFN2/LC3/TSPO and facilitating apoptosis. ACOT11 functions as a PCa tumor suppressor by disrupting mitochondrial homeostasis and blocking PI3K/AKT, serving as a promising CRPC biomarker and therapeutic target.

1.INTRODUCTION

Prostate cancer (PCa) is one of the most common malignant tumors in men worldwide, with high morbidity and mortality In recent years, the incidence of PCa in China has increased rapidly. Although early stage PCa has a favorable prognosis, most patients gradually progress to castration resistant prostate cancer (CRPC) within 2 years, which is accompanied by rapid progression, distant metastasis and poor prognosis[1]. Therefore, exploring the molecular mechanisms underlying the occurrence and development of PCa and identifying effective therapeutic targets are of great clinical significance.

Metabolic reprogramming is an important hallmark of malignant tumors. A large number of studies have confirmed that lipid metabolism disorder and mitochondrial dysfunction are closely related to the malignant progression of PCa[2], [3]. PCa cells undergo significant metabolic remodeling, including enhanced fatty acid synthesis and abnormal mitochondrial energy supply, which provide sufficient materials and energy for tumor proliferation, migration and invasion. Acyl CoA thioesterases (ACOTs) are key enzymes that maintain lipid metabolism balance by hydrolyzing acyl CoA[4]. As an important member of the ACOT family, ACOT11 is mainly located in peroxisomes and participates in the hydrolysis of long chain fatty acyl CoA, thus regulating lipid metabolism, mitochondrial function and cell signal transduction[4], [5].Previous studies have shown that ACOT11 exhibits different expression patterns and biological functions in various tumors. ACOT11 is highly expressed in lung cancer and promotes tumor progression[6], [7], while it is lowly expressed in renal cancer and acts as a tumor suppressor[8]. However, the expression and role of ACOT11 in PCa have not been fully elucidated. The present study hypothesized that ACOT11 may affect the biological behavior of PCa cells by regulating mitochondrial function and the PI3K/AKT signaling pathway[9]. Therefore, the present study detected the expression of ACOT11 in PCa tissues and cell lines, explored its effects on proliferation, migration, invasion and

apoptosis of PCa cells, and further investigated its underlying molecular mechanism, aiming to provide a new theoretical basis and potential target for the diagnosis and treatment of PCa.

2.MATERIALS AND METHODS

Patients and tissue samples

A total of 20 patients with PCa and 20 patients with benign prostatic hyperplasia (BPH) who underwent surgery at Shijiazhuang People's Hospital between March 2021 and March 2023 were enrolled in the present study. The inclusion criteria were as follows: i) Pathologically confirmed primary PCa or BPH; ii) no preoperative androgen deprivation therapy, chemotherapy or radiotherapy; iii) complete clinical data. The exclusion criteria were as follows: i) recurrent PCa; ii) combined with other malignant tumors, severe liver and kidney dysfunction or immune system diseases. The present study was approved by the Medical Ethics Committee of Shijiazhuang People's Hospital (approval no. 2025 109). Written informed consent was obtained from each patient. (i) identifying the institutional and licensing committee approving the experiments, including any relevant details; (ii) confirming that all experiments were performed in accordance with relevant guidelines and regulations.

Cell culture and transfection

Human prostate cancer cell lines including DU145 (Procell, CL-0075), PC-3 (Procell, CL-0185), 22RV1 (Procell, CL-0004), and malignantly transformed prostate epithelial cell line RWPE-2 (QiShi Bio, 7-1391) were used in this study. For cell resuscitation, cryovials were retrieved from liquid nitrogen and immediately thawed in a 37°C constant-temperature water bath (Chunlan Meibiao, HH-US-B). After centrifugation, cells were resuspended and seeded into T25 culture flasks (Costar, 430639), followed by incubation in a humidified incubator (Panasonic, MCO-18AC) at 37°C with 5% CO_2.

Cells were routinely cultured in corresponding complete media: RPMI-1640 medium (Procell, PM150110) for DU145 and 22RV1 cells, Ham's F-12K medium (Procell, PM150910) for PC-3 cells, and MEM medium supplemented with non-essential amino acids (NEAA) (Procell, PM150410) for RWPE-2 cells. All media were supplemented with 10% fetal bovine serum (Sijiqing, 11011 – 8611) and 1% penicillin-streptomycin mixture (Solarbio, P1400). When cell confluence reached 70%–80%, cells were digested with trypsin (Solarbio, T8150), centrifuged at 1500 rpm for 5 min using a low-speed centrifuge (Beili, LDZ5-2), and then subcultured. For cell cryopreservation, the freezing medium was prepared with basal medium, fetal bovine serum and DMSO at a volume ratio of 5:4:1. Cells were preserved long-term in liquid nitrogen after gradient cooling.

All transfection experiments were performed in a biological safety cabinet (Hujing, SW-CJ-1FD). Taking 6-well plates as an example, cells were seeded at a density of 5×10^5 cells per well 24 h prior to transfection, and transfection was performed when cell confluence reached 50%–80%. For overexpression plasmid transfection, 4 μg of ACOT11 overexpression plasmid (GenePharma) and 8 μL of TransIntro EL transfection reagent (TransGen Biotech, FT201-01) were separately diluted in OPTI-MEM

medium (GIBCO, 31985-062). The diluted solutions were mixed gently and incubated at room temperature for 20 min to form transfection complexes. For siRNA transfection, 250 pmol of ACOT11 siRNA (GenePharma) and 10 μL of TransIntro EL transfection reagent were used to prepare complexes following the same protocol. The prepared transfection complexes were added dropwise to the cell culture medium. After incubation at 37°C for 4–6 h, the medium was replaced with fresh complete medium. Cells were harvested at 48 h post-transfection for subsequent experimental analyses.

Tissue Reverse transcription quantitative PCR (RT qPCR)

A total of 20 prostate cancer tissues (tumor 1–20) and 20 matched normal prostate tissues (normal 1–20) were enrolled in this study. Total RNA was extracted from tissue samples using Trizol reagent (Cat# 15596-026, Invitrogen). Briefly, an appropriate amount of tissue was fully lysed in 1 mL Trizol solution, followed by the addition of 0.2 mL chloroform (Yongda Chemical Reagent Co., Ltd.). The mixture was centrifuged at 12,000 rpm for 15 min at 4°C using an Eppendorf 5415D centrifuge, and the upper aqueous phase was carefully collected. Subsequently, 0.5 mL isopropanol (Yongda Chemical Reagent Co., Ltd.) was added to precipitate RNA. After incubation on ice for 10 min, the sample was centrifuged again. The supernatant was discarded, and the RNA precipitate was washed with 75% anhydrous ethanol (Yongda Chemical Reagent Co., Ltd.), followed by centrifugation at 12,000 rpm for 5 min at 4°C. The dried RNA precipitate was dissolved in DEPC-treated water (Solarbio Science & Technology Co., Ltd.). The concentration and purity of total RNA were determined using a Denovix DS-11 ultra-micro spectrophotometer, and samples with an absorbance ratio (260/280 nm) ranging from 1.8 to 2.1 were included for subsequent experiments.

Subsequently, cDNA was synthesized using the HiFiScript gDNA Removal cDNA Synthesis Kit (Cat# CW2582M, CWBio). Genomic DNA was eliminated by incubation with gDNA Eraser at 42°C for 2 min. First-strand cDNA was synthesized with Oligo-dT primers at 42°C for 15 min, followed by incubation at 85°C for 5 min. ACTIN was used as an internal reference gene for quantitative analysis. Quantitative PCR was performed on a Bio-Rad CFX Connect™ real-time fluorescence quantitative PCR instrument using MonAmp SYBR Green qPCR Mix (Cat# MQ00401S, Monad Biotech). The 20 μL reaction system contained 10 μL of 2× SuperReal PreMix Plus, 0.6 μL of forward and reverse primers (10 μM), 100 ng of cDNA template, and nuclease-free water to adjust the final volume. The amplification procedure was set as follows: initial denaturation at 95°C for 15 min, followed by 40 cycles of denaturation at 95°C for 10 s, annealing at 53–58°C for 30 s, and extension at 72°C for 30 s. Melting curve analysis was performed from 60°C to 95°C after amplification. Each sample was analyzed in triplicate. The relative mRNA expression level of ACOT11 was calculated using the 2 method with blank controls as the reference.

Cell Reverse Transcription-Quantitative Polymerase Chain Reaction (RT-qPCR)

Total RNA was extracted from human prostate cancer cells (PC-3, 22RV1, DU145) and malignantly transformed prostate epithelial RWPE-2 cells using Trizol reagent (Cat# 15596-026, Invitrogen). Briefly, 1×10^6 to 1×10^7 cells were fully lysed in 1 mL Trizol reagent. Then, 0.2 mL chloroform was added, and the mixture was centrifuged to collect the upper aqueous phase. RNA was precipitated with isopropanol,

washed with 75% anhydrous ethanol, and dissolved in DEPC-treated water (Solarbio Science & Technology Co., Ltd.) after air drying. The concentration and purity of extracted RNA were detected using a Denovix DS-11 ultra-micro spectrophotometer. Subsequently, cDNA was synthesized utilizing the HiFiScript gDNA Removal cDNA Synthesis Kit (Cat# CW2582M, CWBio). Genomic DNA was eliminated with gDNA Eraser, and first-strand cDNA was synthesized using Oligo-dT primers.

ACTIN was applied as an internal reference gene. Quantitative PCR amplification was performed on a Bio-Rad CFX Connect™ real-time fluorescence quantitative PCR instrument using MonAmp SYBR Green qPCR Mix (Cat# MQ00401S, Monad Biotech). The 20 μL reaction system consisted of 10 μL 2× SuperReal PreMix Plus, 0.6 μL of forward and reverse primers (10 μM), 100 ng cDNA template, and nuclease-free water to supplement the volume. The amplification conditions were as follows: initial denaturation at 95°C for 15 min, followed by 40 cycles of 95°C for 10 s, 53–58°C for 30 s, and 72°C for 30 s. Melting curve analysis was conducted after amplification. Each sample was tested in triplicate. The relative mRNA expression level of ACOT11 was quantified by the 2 method, with PC-3 cells serving as the control group. The primer sequences used in this experiment were listed as follows: ACOT11 (forward: 5'-GCGATCTGGAGAGCAGAGAC-3', reverse: 5'-GTGGCCACATTCTCCATCCA-3'); ACTIN (forward: 5'-AAGGAGCCCCACGAGAAAAAT-3', reverse: 5'-ACCGAACTTGCATTGATTCCAG-3').

Western blotting

After cell collection, total protein was extracted using RIPA lysis buffer (Cat# R0020, Solarbio) on ice. The protein concentration was quantified with a Denovix DS-11 ultra-micro spectrophotometer. Protein samples were mixed with loading buffer and denatured at 95°C for 10 min. Subsequently, SDS-PAGE electrophoresis was performed using a JY-SCZ4 + electrophoresis system at a constant voltage of 150 V until the target bands migrated to two-thirds of the separating gel. Proteins were transferred onto Millipore PVDF membranes (Cat# IPVH00010) using an ATTO semi-dry transfer system at a constant current of 250 mA for 40 min. After transfer, the membranes were blocked with 5% skimmed milk at room temperature for 2 h. The membranes were then incubated with primary antibodies against ACOT11 (10776-1-AP, Proteintech, 1:1000) and β-Actin (66009-1-Ig, Proteintech, 1:30000) overnight at 4°C. Following washing with PBST, the membranes were incubated with corresponding secondary antibodies, including goat anti-rabbit IgG (ZB2301, ZSGB-BIO) and goat anti-mouse IgG (ZB2305, ZSGB-BIO), at room temperature for 90 min. Protein bands were visualized using a Bioss ECL chemiluminescence kit (Cat# C05-07004), and images were captured with a Tanon 4800 chemiluminescence imaging system. Thermo pre-stained protein markers (Cat# 26617) were used to indicate protein molecular weights. The grayscale value of each band was analyzed using the supporting imaging software.

Cell Counting Kit 8 (CCK 8) assay

Cells were seeded into 96 well plates at a density of 5,000 cells/well. At 0, 24, 48 and 72 h, 10 μl CCK 8 solution was added to each well and incubated for 2 h. The absorbance at 450 nm was detected using a microplate reader to evaluate cell proliferation ability.

Cell Wound Healing Assay

DU145 (oe NC, oe ACOT11) and PC 3 (si NC, si ACOT11) cells in the logarithmic growth phase were seeded in 6-well plates (3516, Costar). When the cell confluence reached 80%, a sterile 200 μL pipette tip was used to create uniform vertical scratches along the marked lines on the bottom of the plates. The detached cellular debris was removed by gentle washing with PBS, and the cells were subsequently cultured in serum-free medium in a humidified incubator (MCO 18AC, Panasonic) containing 5% CO_2 at 37°C. Microscopic images were captured at 0 h and 48 h after scratching using an inverted microscope (IX71, OLYMPUS). The wound healing area of each group was compared to evaluate the migratory capacity of prostate cancer cells.

Transwell invasion assay

Matrigel matrix gel (Cat# 356234, BD) was thawed overnight at 4°C before the experiment. Subsequently, the gel was diluted with serum-free medium at a ratio of 1:8 on ice. A total of 50 μL of the diluted Matrigel was evenly added into the upper chamber of Transwell inserts (Cat# 3422, Costar) and incubated at 37°C for 30 min to allow coagulation. DU145 (oe NC, oe ACOT11) and PC 3 (si NC, si ACOT11) cells in the logarithmic growth phase were resuspended in serum-free medium, and the cell density was adjusted to 2×10^4 cells/200 μL. The cell suspension was seeded into the upper chamber, while 600 μL of complete medium was added to the lower chamber as a chemotactic inducer. The cells were incubated in a humidified incubator (MCO 18AC, Panasonic) with 5% CO_2 at 37°C for 48 h. After incubation, the cells were washed with PBS and fixed at room temperature for 20 min. The membranes were stained with crystal violet staining solution (Cat# G1063, Solarbio) for 20 min. The non-invasive cells remaining on the upper surface of the membrane were gently wiped off with a cotton swab. Finally, the invasive cells were observed and photographed under an inverted microscope (IX71, OLYMPUS), and the number of penetrated cells was counted to evaluate cell invasive ability.

Cell Counting Kit-8 (CCK-8) Assay

DU145 (oe NC, oe ACOT11) and PC 3 (si NC, si ACOT11) cells in the logarithmic growth phase were seeded in 96-well plates (Cat# 3599, Costar) at a density of 5000 cells per well in a volume of 100 μL. Three replicate wells were set for each group at every time point. The plates were incubated in a humidified incubator (MCO 18AC, Panasonic) containing 5% CO_2 at 37°C. At 0 h, 24 h, 48 h, and 72 h after cell adherence, 10 μL of CCK-8 detection reagent (Cat# CA0038, Beyotime) was added to each well, and the plates were further incubated for 2 h. The absorbance value of each well at a wavelength of 450 nm (OD_{450}) was measured using a microplate reader (Varioskan LUX, Thermo), and the absorbance values were used to reflect cell proliferative activity.

Flow Cytometry Detection

DU145 (oe NC, oe ACOT11) and PC 3 (si NC, si ACOT11) cells in the logarithmic growth phase were harvested using a low-speed centrifuge (LDZ5-2, Beili) after treatment, and subsequent detection was

performed via a flow cytometer (Attune NXT, Thermo). For cell apoptosis detection, an Annexin V/PI apoptosis detection kit (Cat# C1062S, Beyotime) was used. Cells were washed with PBS and resuspended in Annexin V-FITC binding buffer, followed by staining with Annexin V-FITC and PI. After incubation for 10 min at room temperature in the dark, the samples were detected. The blank tube was used for voltage adjustment, and single-stained tubes were applied for compensation calibration. Fluorescence signals were collected through the BL-1 and BL-2 channels. A JC-1 enhanced mitochondrial membrane potential detection kit (Cat# C2003S, Beyotime) was utilized for mitochondrial membrane potential measurement. Cells were resuspended in 200× JC-1 working solution and incubated at 37°C for 20 min before detection after washing. For intracellular reactive oxygen species (ROS) measurement, a ROS detection kit (Cat# S0035S, Beyotime) was adopted. Cells were incubated with serum-free medium containing 5 μM CM-H2DCFDA at 37°C for 30 min and washed prior to detection. Mitochondrial superoxide was detected using a mitochondrial superoxide detection kit (Cat# S0061S, Beyotime). Cells were incubated with 5 μM MitoSOX working solution at 37°C for 30 min, followed by washing and detection. Mitochondrial calcium levels were measured using the fluorescent calcium probe Rhod-2 AM (HY-D0989, MCE). Cells were resuspended in 5 μM Rhod-2 AM working solution and incubated at room temperature for 15 min, then washed with PBS for subsequent detection. The blank unstained tubes were used for voltage calibration in all flow cytometry assays. All data were exported for further statistical analysis after detection.

ATP Detection Assay

DU145 (oe NC, oe ACOT11) and PC 3 (si NC, si ACOT11) cells in the logarithmic growth phase were collected after treatment. Protein quantification was performed using a BCA Protein Assay Kit (Cat# P0012S, Beyotime). Briefly, the 20 mg/mL protein standard was diluted to a working concentration of 2 mg/mL. BCA reagent A and reagent B were mixed at a volume ratio of 50:1 to prepare the working solution. A total of 20 μL of standards and samples were added into 96-well plates (Cat# 3599, Costar), followed by the addition of 200 μL BCA working solution per well. After incubation at 37°C for 30 min, the absorbance at 562 nm was measured using a multifunctional microplate reader (Varioskan LUX, Thermo). A standard curve was plotted to calculate the protein concentration of each sample. An Enhanced ATP Assay Kit (Cat# S0027, Beyotime) was utilized for ATP measurement. Briefly, 100 μL of ATP detection working solution was added to each well and incubated at room temperature for 3–5 min to eliminate background interference. Subsequently, 20 μL of samples or standards were supplemented and mixed rapidly. The relative light unit (RLU) was detected using a multifunctional microplate reader. The ATP concentration was calculated according to the standard curve, and the final ATP content was normalized to the protein concentration and presented as nmol/mg protein. All experimental operations were conducted in a biosafety cabinet (SW CJ 1FD, Hujing), and cells were cultured in a humidified incubator (MCO 18AC, Panasonic) with 5% CO_2 at 37°C.

Transmission electron microscopy (TEM)

Cells were initially fixed with 2.5% glutaraldehyde (18427, Ted Pella Inc) at 4°C for 2–4 h. After rinsing three times with 0.1 M phosphate buffer for 15 min per rinse, the cells were post-fixed with 1% osmium tetroxide (18456, TED PELLA) at 4°C for 4 h or overnight. Subsequently, the samples were subjected to gradient dehydration with serially concentrated anhydrous ethanol (100092183, Sinopharm Chemical Reagent Co., Ltd.), including 30%, 50%, 70%, 80%, 95%, and 100% ethanol for 40 min at each concentration. The samples were then treated with propylene oxide (80059118, Sinopharm Chemical Reagent Co., Ltd.) three times for 30 min each. After dehydration, gradient infiltration and embedding were performed using an Epond-812 embedding resin kit (18010, TED PELLA). The embedded samples were polymerized in an oven at 60°C for 48 h. After polymerization, ultrathin sections of 70 nm were prepared using a Leica UC7 ultramicrotome equipped with a Daitome Ultra 45° diamond knife. The sections were mounted on 150-mesh copper grids (AZH150, Zhongjingkeyi Technology Co., Ltd.). The sections were sequentially stained with 3% uranyl acetate (22400, EMS) for 8 min and 2.7% lead citrate (HD17810) for 8 min. After washing and air-drying, the cellular ultrastructure was observed and imaged using a JEOL JEM1400 transmission electron microscope.

Bioinformatics analysis

RNA seq data of PCa were downloaded from The Cancer Genome Atlas (TCGA) database. Differential expression analysis and KEGG pathway enrichment analysis were performed using R software to predict the potential signaling pathway regulated by ACOT11[10], [11].

Statistical analysis

Bioinformatics Analysis:

1. 1. Data Acquisition: This study utilized the public database The Cancer Genome Atlas (TCGA) to investigate the expression level and clinical significance of acyl-CoA thioesterase 11 (ACOT11) in prostate cancer. Standardized RNA-Seq transcriptome data (FPKM values) and corresponding clinicopathological information of the Prostate Adenocarcinoma (PRAD) project were downloaded from TCGA data (https://portal.gdc.cancer.gov/). The final dataset included cancer tissue samples and paired/adjacent normal tissue samples for subsequent comparative analysis.
2. 2. Differential Expression Analysis: R language (v4.2.0) and the DESeq2 package were used to perform Gene Ontology (GO) and Kyoto Encyclopedia of Genes and Genomes (KEGG) enrichment analyses on the expression level of ACOT11. The criteria for judging the significance of mitochondrial-related differential expression of ACOT11 between cancer and normal tissues were $|\log2(\text{Fold Change})| > 1$ and false discovery rate (FDR)-adjusted P value (adj. P) < 0.05.
3. 3. Statistical Analysis: All statistical analyses were performed in the R environment. The Wilcoxon test was used for comparisons between groups. A P value < 0.05 was considered statistically significant.

3.RESULTS

ACOT11 is downregulated in PCa tissues and cell lines

RT-qPCR Results of Tissue Samples

The mRNA expression level of ACOT11 in 20 prostate cancer tissues and 20 normal prostate tissues was detected by reverse transcription-quantitative polymerase chain reaction (RT-qPCR). ACTIN was used as an internal reference gene, and the 2 method was applied for relative quantitative analysis. The results showed that the relative expression level of ACOT11 in prostate cancer tissues was 1.21, which was significantly lower than that in normal prostate tissues (2.00). Compared with normal prostate tissues, ACOT11 was markedly downregulated in prostate cancer tissues, and the difference was statistically significant ($P < 0.05$). These findings indicated that the low expression of ACOT11 was closely correlated with the occurrence and progression of prostate cancer.

RT-qPCR Results of Cell Lines

The mRNA expression levels of ACOT11 in prostate epithelial cells and different prostate cancer cell lines were determined by RT-qPCR. Relative quantification was performed using the 2 method with PC-3 cells as the control group. The relative expression level of ACOT11 was 0.717 in normal prostate epithelial RWPE-2 cells, 0.382 in 22Rv1 cells, and 0.282 in DU145 cells. Compared with PC-3 cells, the expression of ACOT11 was significantly decreased in RWPE-2, 22Rv1, and DU145 cells, with the lowest expression observed in DU145 cells. The differences among groups were statistically significant ($P < 0.05$). These results suggested that the low expression of ACOT11 was closely associated with the malignant phenotype of prostate cancer cells.

Interference Efficiency Detection of ACOT11 siRNA

The mRNA expression level of ACOT11 in cells transfected with ACOT11 small interfering RNA (siRNA) was measured by RT-qPCR. Relative quantitative analysis was conducted using the 2 method with the siNC negative control group as the reference. The relative expression level of ACOT11 was 0.267 in the si-ACOT11-1 group, 0.143 in the si-ACOT11-2 group, and 0.639 in the si-ACOT11-3 group. Compared with the siNC group, all three siRNA sequences significantly downregulated the expression of ACOT11. Among them, si-ACOT11-2 exhibited the highest interference efficiency. The differences were statistically significant ($P < 0.01$), so si-ACOT11-2 was selected for subsequent cell functional experiments.

Identification of ACOT11 Knockdown and Overexpression Cell Models

RT-qPCR was performed to detect the mRNA expression levels of target genes in PC-3 cells with ACOT11 knockdown and DU145 cells with ACOT11 overexpression. Relative quantification was analyzed via the 2 method using the corresponding negative control groups as references. In PC-3 cells, the relative expression level of ACOT11 in the si-ACOT11 group was 0.149, which was markedly decreased compared with the siNC group. In DU145 cells, the relative expression level of ACOT11 in the oe-ACOT11 group was 13.027, which was significantly higher than that in the oe-NC group. Both knockdown and

overexpression exhibited ideal transfection efficiency with statistically significant differences ($P < 0.001$), which met the requirements for subsequent functional experiments.

Western blot was used to determine the protein expression levels of ACOT11 in knockdown and overexpression cell models, with β-Actin serving as an internal reference. Grayscale quantitative analysis demonstrated that the protein level of ACOT11 was significantly downregulated in the si-ACOT11 group compared with the siNC group, while it was prominently upregulated in the oe-ACOT11 group relative to the oe-NC group. The differences in protein expression among all groups were statistically significant ($P < 0.001$). These results indicated that ACOT11 knockdown and overexpression cell models were successfully constructed and could be applied for subsequent functional experiments.

Effect of ACOT11 on Cell Proliferation

The CCK-8 assay was performed to evaluate the effect of ACOT11 on the proliferative capacity of prostate cancer cells. In DU145 cells, the proliferation rate of the oe-ACOT11 overexpression group was significantly decreased compared with the oe-NC control group, with the most obvious differences observed at 48 h and 72 h. In PC-3 cells, the proliferation rate was markedly increased in the si-ACOT11 knockdown group relative to the si-NC control group. The differences between groups at each time point were statistically significant ($P < 0.05$). These results suggested that ACOT11 could significantly inhibit the proliferation of prostate cancer cells.

Effect of ACOT11 on Cell Invasion

A cell wound healing assay was performed to evaluate the effect of ACOT11 on the migration ability of prostate cancer cells. At 48 h after scratching, the wound healing rate of the oe-ACOT11 overexpression group was significantly reduced compared with the oe-NC group in DU145 cells, indicating an attenuated migratory capacity. In PC-3 cells, the si-ACOT11 knockdown group showed a higher wound healing rate and enhanced migration ability relative to the si-NC group. The differences between each experimental group and the corresponding control group were statistically significant ($P < 0.05$). These results suggested that ACOT11 could significantly inhibit the migration of prostate cancer cells.

Transwell invasion assay was conducted to explore the effect of ACOT11 on the invasive ability of prostate cancer cells. In DU145 cells, the number of cells penetrating the Matrigel was significantly lower in the oe-ACOT11 overexpression group than in the oe-NC group, indicating weakened invasive capacity. In PC-3 cells, the si-ACOT11 knockdown group exhibited a markedly increased number of invasive cells compared with the si-NC group, which suggested enhanced invasive ability. The differences between the experimental groups and their corresponding control groups were statistically significant ($P < 0.01$). These findings indicated that ACOT11 could remarkably suppress the invasion of prostate cancer cells.

Flow cytometry was used to simultaneously detect cell apoptosis, mitochondrial membrane potential, intracellular total reactive oxygen species (ROS), mitochondrial ROS (mtROS), and mitochondrial calcium ($mtCa^{2+}$) levels. The results showed that in DU145 cells, compared with the oe NC control group, the oe

ACOT11 overexpression group presented a significantly higher apoptosis rate, a marked reduction in mitochondrial membrane potential, and remarkably elevated levels of total ROS, mtROS and mitochondrial Ca^{2+}. In PC 3 cells, relative to the si NC control group, the si ACOT11 knockdown group exhibited a significantly lower apoptosis rate, an obvious increase in mitochondrial membrane potential, and distinctly decreased levels of total ROS, mtROS and mitochondrial Ca^{2+}. The differences in the above indexes between each group and the corresponding control group were statistically significant ($P<0.05$), suggesting that ACOT11 could induce the apoptosis of prostate cancer cells by regulating mitochondrial homeostasis.

An enhanced ATP detection kit combined with BCA protein quantification was used to detect the effect of ACOT11 on energy metabolism in prostate cancer cells. The results showed that the intracellular ATP content was significantly decreased in the oe-ACOT11 overexpression group compared with the oe-NC control group in DU145 cells. In PC-3 cells, the intracellular ATP content was remarkably increased in the si-ACOT11 knockdown group relative to the si-NC control group. The differences between each experimental group and the corresponding control group were statistically significant ($P < 0.01$). These results suggested that ACOT11 could significantly inhibit energy synthesis and participate in the regulation of mitochondrial metabolic function in prostate cancer cells.

Transmission electron microscopy (TEM)

Transmission electron microscopy was performed to observe the effect of ACOT11 on the ultrastructure of prostate cancer cells. The results showed that compared with the control group, the oe-ACOT11 overexpression group exhibited typical apoptotic characteristics, including obviously swollen mitochondria, fractured or disappeared mitochondrial cristae, and disordered internal structures. In contrast, the si-ACOT11 knockdown group maintained relatively intact mitochondrial morphology with clear structure, and the ultrastructural alterations related to apoptosis were notably alleviated. Significant differences in mitochondrial structure and apoptotic morphology were observed among groups ($P < 0.05$). These findings further confirmed that ACOT11 could induce prostate cancer cell apoptosis by disrupting mitochondrial structural homeostasis.

ACOT11 inactivates the PI3K/AKT signaling pathway

KEGG pathway enrichment analysis.

Top 20 significantly enriched pathways are shown. The PI3K-Akt signaling pathway is highlighted as one of the most significantly enriched pathways. The GeneRatio (x-axis), number of genes (bubble size), and adjusted p-value (color gradient) are indicated.

RT-qPCR was performed to detect the regulatory effect of ACOT11 on the mRNA expression levels of LC3, TSPO, MFN2, PI3K, and AKT. In PC-3 cells, the mRNA levels of LC3 and MFN2 were significantly decreased, while TSPO, PI3K, and AKT were markedly upregulated in the si-ACOT11 knockdown group compared with the siNC group. In DU145 cells, the oe-ACOT11 overexpression group exhibited elevated

expression of LC3 and MFN2, along with reduced levels of TSPO, PI3K, and AKT relative to the oe-NC group. The differences in gene expression between each experimental group and matched control group were statistically significant ($P < 0.05$). These results indicated that ACOT11 exerts tumor-suppressive effects by modulating the PI3K/AKT signaling pathway, as well as the expression of genes related to mitochondrial fusion and autophagy.

Western blot was used to detect the expression levels of related proteins. Grayscale quantitative analysis demonstrated that in PC-3 cells, the LC3-II/LC3-I ratio and MFN2 protein expression were significantly decreased, whereas the levels of TSPO and the ratios of p-PI3K/PI3K and p-AKT/AKT were markedly increased in the si-ACOT11 knockdown group compared with the siNC group. In DU145 cells, the oe-ACOT11 overexpression group presented an increased LC3-II/LC3-I ratio and higher MFN2 expression, while the levels of TSPO, p-PI3K/PI3K and p-AKT/AKT were distinctly reduced relative to the oe-NC group. The differences in protein expression among all groups were statistically significant ($P < 0.05$). These data indicated that ACOT11 could inhibit the activation of the PI3K/AKT signaling pathway and regulate the expression of proteins associated with mitochondrial fusion and autophagy.

4. DISCUSSION

As an important member of the acyl-CoA thioesterase family, ACOT11 is mainly involved in the hydrolysis of long-chain acyl-CoA and the regulation of lipid metabolic homeostasis, and plays a pivotal role in tumor metabolic reprogramming[4]. Accumulating studies have revealed that ACOT11 exhibits functional heterogeneity across various tumors: it is highly expressed and exerts oncogenic effects in lung cancer[6], [7], while it is downregulated and possesses tumor-suppressive potential in renal cell carcinoma[8]. This study systematically elucidates for the first time the expression patterns, biological functions and molecular mechanisms of ACOT11 in prostate cancer. We confirm that ACOT11 acts as a tumor suppressor gene to restrain the malignant progression of prostate cancer via regulating the PI3K/AKT signaling pathway and mitochondrial homeostasis[3], which provides novel experimental evidence and theoretical basis for metabolic targeted therapy of prostate cancer.

In this study, analyses of clinical samples, cell lines, and the TCGA database confirmed that ACOT11 was significantly downregulated in prostate cancer tissues compared with adjacent normal tissues, with the lowest expression level detected in highly invasive DU145 cells. These findings suggest that low ACOT11 expression is negatively correlated with the malignant degree and metastatic potential of prostate cancer. Consistent with the expression trend of ACOT11 observed in renal cell carcinoma but contrary to that in lung cancer, this result indicates that ACOT11 exhibits distinct tumor type-specific functions. Bioinformatics analysis demonstrated that the differentially expressed genes associated with ACOT11 were markedly enriched in mitochondrial energy metabolism, fatty acid metabolism, and the PI3K/AKT signaling pathway[3], [9], providing critical directions for the mechanistic exploration of the present study.

Mitochondrial homeostasis imbalance is a core hallmark of tumor metabolic reprogramming, and ACOT11 can directly regulate mitochondrial structure and function[4], [12]. In the present study, ACOT11 overexpression reduced mitochondrial membrane potential, inhibited ATP production, elevated mitochondrial ROS and Ca^{2+} levels, and induced typical apoptotic ultrastructural changes including mitochondrial swelling and cristae fragmentation[2], [13]. Conversely, ACOT11 knockdown maintained intact mitochondrial morphology and enhanced cellular energy metabolism. These results demonstrate that ACOT11 induces prostate cancer cell apoptosis by disrupting mitochondrial homeostasis. This study firstly establishes a direct link between the ACOT11-mitochondrial metabolic axis and the regulation of prostate cancer apoptosis, and further improves the theoretical system of tumor progression driven by lipid metabolic disorder.

At the signaling pathway level, the present study confirmed that ACOT11 negatively regulates the PI3K/AKT signaling pathway and significantly decreases the ratios of p-PI3K/PI3K and p-AKT/AKT[3]. The PI3K/AKT pathway is abnormally activated in prostate cancer and is closely associated with cell proliferation, anti-apoptosis, invasion, metastasis, and castration resistance[1]. The AKT inhibitor MK-2206 significantly reversed the malignant phenotypes mediated by ACOT11 knockdown, indicating that PI3K/AKT serves as a critical downstream effector pathway of ACOT11. Combined with the expression changes of mitochondrial fusion and autophagy-related molecules such as MFN2, LC3, and TSPO[13], [14], this study initially constructed a regulatory pattern of the ACOT11–PI3K/AKT–mitochondrial metabolic axis, providing a comprehensive mechanistic explanation spanning lipid metabolism, signaling pathways, and mitochondrial function.

The present study suggests that low ACOT11 expression can serve as a potential molecular biomarker for poor prognosis and high metastatic risk in prostate cancer, providing a novel indicator for clinical stratification and precise treatment. Restoration of ACOT11 expression or targeted inhibition of the PI3K/AKT pathway may represent a promising metabolic therapeutic strategy for prostate cancer, particularly for castration-resistant prostate cancer (CRPC)[1]. Compared with single-dimensional studies, this research integrates lipid metabolism, mitochondrial function, and classical oncogenic signaling pathways, which better reflects the actual regulatory network of tumors and possesses important theoretical value and translational prospects.

Nevertheless, several limitations of this study should be acknowledged. First, only in vitro cellular experiments were performed without verification using in vivo animal models. Second, large-sample clinical cohorts and long-term survival analyses were not conducted. Third, the upstream regulatory mechanism of ACOT11 and the direct molecular interaction between ACOT11 and the PI3K/AKT pathway remain to be further elucidated. Future studies will focus on the above aspects to further promote the potential of ACOT11 as a novel diagnostic and therapeutic target for prostate cancer.

Conclusion

The present study systematically explored the expression characteristics, biological functions, and molecular regulatory mechanisms of ACOT11 in prostate cancer cells. The intrinsic tumor-suppressive mechanism of ACOT11 was elucidated from the perspective of the crosstalk among lipid metabolism disturbance, mitochondrial homeostasis disruption, and aberrant activation of classical signaling pathways. Our findings firstly demonstrated that ACOT11 was markedly downregulated in prostate cancer tissues and highly malignant cell lines. Its expression level was tightly correlated with tumor malignancy, invasive and metastatic potential, and aberrant cell proliferation, indicating that low ACOT11 expression acts as a crucial molecular event during the malignant progression of prostate cancer.

Declarations

ACKNOWLEDGMENTS

The authors greatly thank Wei Li for their support.

AUTHOR CONTRIBUTIONS

Yang Cui : Data curation (equal); formal analysis (equal); investigation (equal); project administration (equal); writing – original draft (lead). Jin Zhao: Data curation (equal); formal analysis (equal); project administration (equal); writing – original draft (equal).He Ran Cao: Data curation (equal); project administration (equal). Wei Li: Data curation (equal).

DATA AVAILABILITY STATEMENT

All raw data and code are available upon request.

CONFLICT OF INTEREST STATEMENT

The authors have no conflict of interest.

FUNDING INFORMATION

NA

ETHICS STATEMENT

Ethical approval was granted by the Ethics Committee of *Shijiazhuang People's Hospital*.

References

1. Role of PI3K-AKT. -mTOR pathway as a pro-survival signaling and resistance-mediating mechanism to therapy of prostate cancer. Accessed: Jun. 01, 2026. [Online]. Available: https://www.mdpi.com/1422-0067/22/20/11088

2. Mitochondrial elongation. and ROS-mediated apoptosis in prostate cancer cells under therapy with apalutamide and complex I inhibitor - PMC. Accessed: Jun. 01, 2026. [Online]. Available: https://pmc.ncbi.nlm.nih.gov/articles/PMC11241170/
3. Chen, L., Xu, Y. X., Wang, Y. S. & Zhou, J. L. Lipid metabolism, amino acid metabolism, and prostate cancer: A crucial metabolic journey, *Asian Journal of Andrology*, vol. 26, no. 2, pp. 123–134, Mar. (2024). 10.4103/aja202363
4. Bai, L., Yang, P., Han, B. & Kong, L. Progress of the acyl-coenzyme a thioester hydrolase family in cancer. *Front. Oncol.* **14**, 1374094. 10.3389/fonc.2024.1374094 (Mar. 2024).
5. Chen, D. et al. Human brown fat inducible thioesterase variant 2 cellular localization and catalytic function, *Biochemistry*, vol. 51, no. 35, pp. 6990–6999, Sep. (2012). 10.1021/bi3008824
6. Hung, J. Y. et al. Overexpression and proliferation dependence of acyl-CoA thioesterase 11 and 13 in lung adenocarcinoma. *Oncol. Lett.* **14** (3), 3647–3656. 10.3892/ol.2017.6594 (Sep. 2017).
7. ACOT11 promotes. cell proliferation, migration and invasion in lung adenocarcinoma - liang - translational lung cancer research. Accessed: Jun. 01, 2026. [Online]. Available: https://tlcr.amegroups.org/article/view/44205/html
8. Xu, C. L. et al. Acyl-CoA thioesterase 8 and 11 as novel biomarkers for clear cell renal cell carcinoma. *Front. Genet.* **11**, 594969. 10.3389/fgene.2020.594969 (Dec. 2020).
9. CMTM5 inhibits the development of prostate cancer via the EGFR/PI3K/AKT signaling pathway - PMC. Accessed: Jun. 01, 2026. [Online]. Available: https://pmc.ncbi.nlm.nih.gov/articles/PMC8628290/
10. Kanehisa, M., Furumichi, M., Sato, Y., Matsuura, Y. & Ishiguro-Watanabe, M. KEGG: Biological systems database as a model of the real world. *Nucleic Acids Res.* **53**, D672–D677. 10.1093/nar/gkae909 (Jan. 2025).
11. Kanehisa, M. KEGG: Kyoto encyclopedia of genes and genomes. *Nucleic Acids Res.* **28** (1), 27–30. 10.1093/nar/28.1.27 (Jan. 2000).
12. Liu, K., Yeh, I., Chou, S., Yen, M. & Kuo, P. Regulatory mechanism of fatty acid–CoA metabolic enzymes under endoplasmic reticulum stress in lung cancer, *Oncol Rep*, Aug. (2018). 10.3892/or.2018.6664
13. VDAC1 and the TSPO. Expression, interactions, and associated functions in health and disease states. Accessed: Jun. 01, 2026. [Online]. Available: https://www.mdpi.com/1422-0067/20/13/3348
14. MFN2 suppresses. cancer progression through inhibition of mTORC2/akt signaling | scientific reports. Accessed: Jun. 01, 2026. [Online]. Available: https://www.nature.com/articles/srep41718

Figures

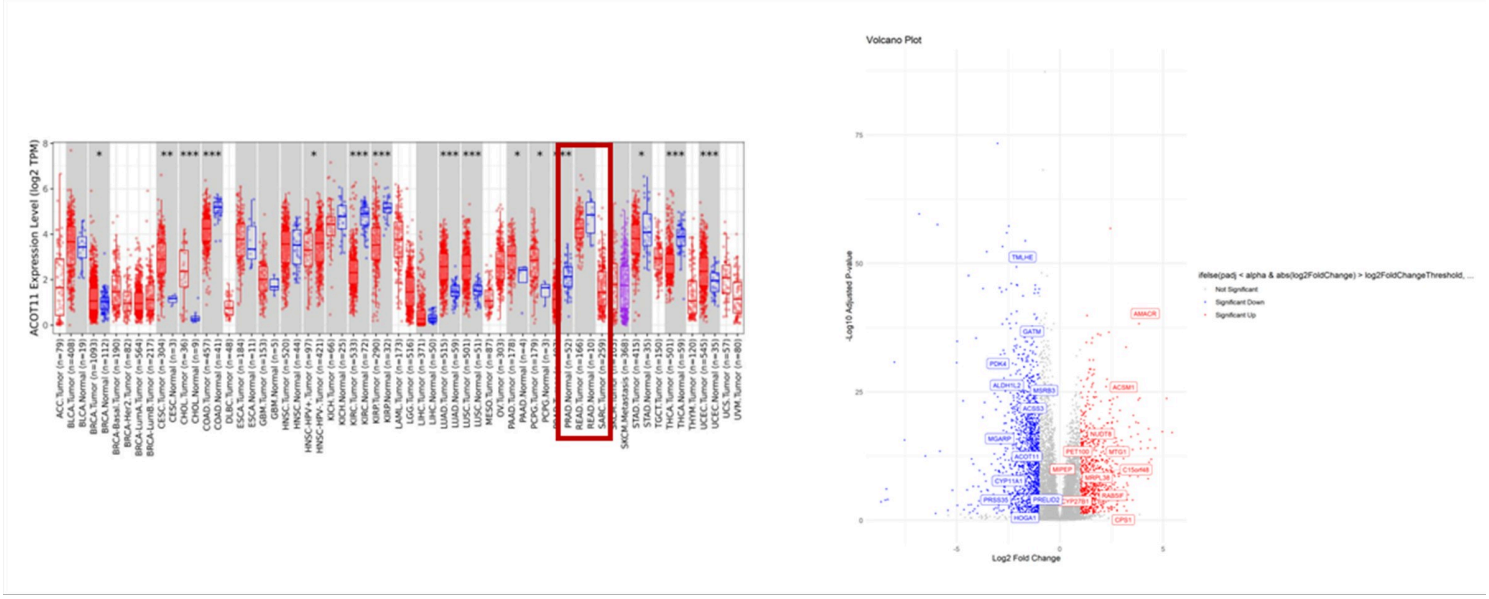


Figure 1

ACOT11 expression across different cancer types in TCGA database.

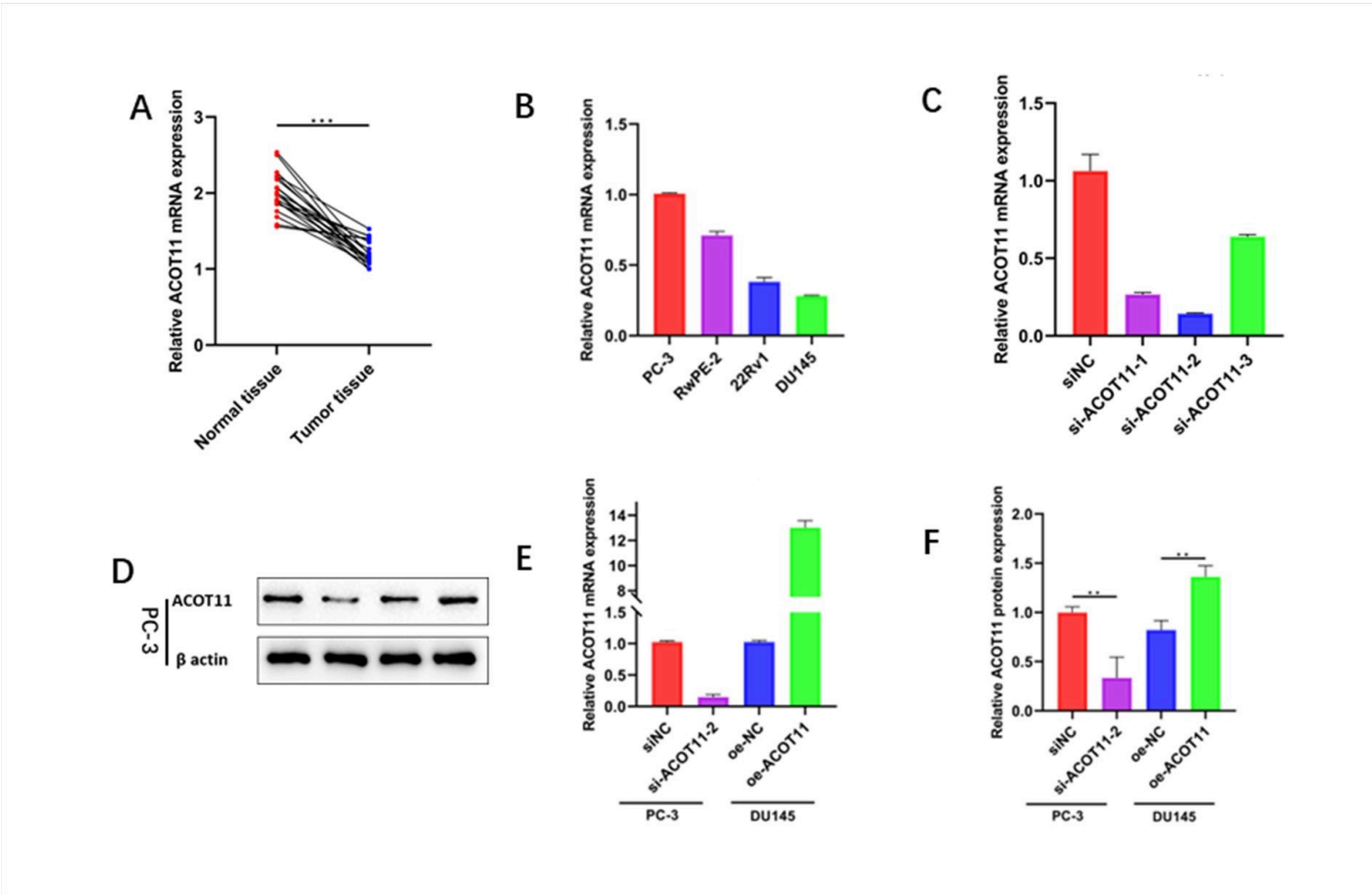


Figure 2

(A) ACOT11 expression in normal tissue and tumor tissue (B) ACOT11 expression in prostate cells PC-3RWPE-2 22Rv1DU145(C) ACOT11 mRNA expression knockdown in PC-3 cells (D) Western blot validation of ACOT11 protein expression in PC-3 cells after siRNA-mediated knockdown and plasmid-mediated overexpression (E) Validation of ACOT11 knockdown and overexpression by RT-qPCR (F) Validation of ACOT11 knockdown and overexpression by WB.

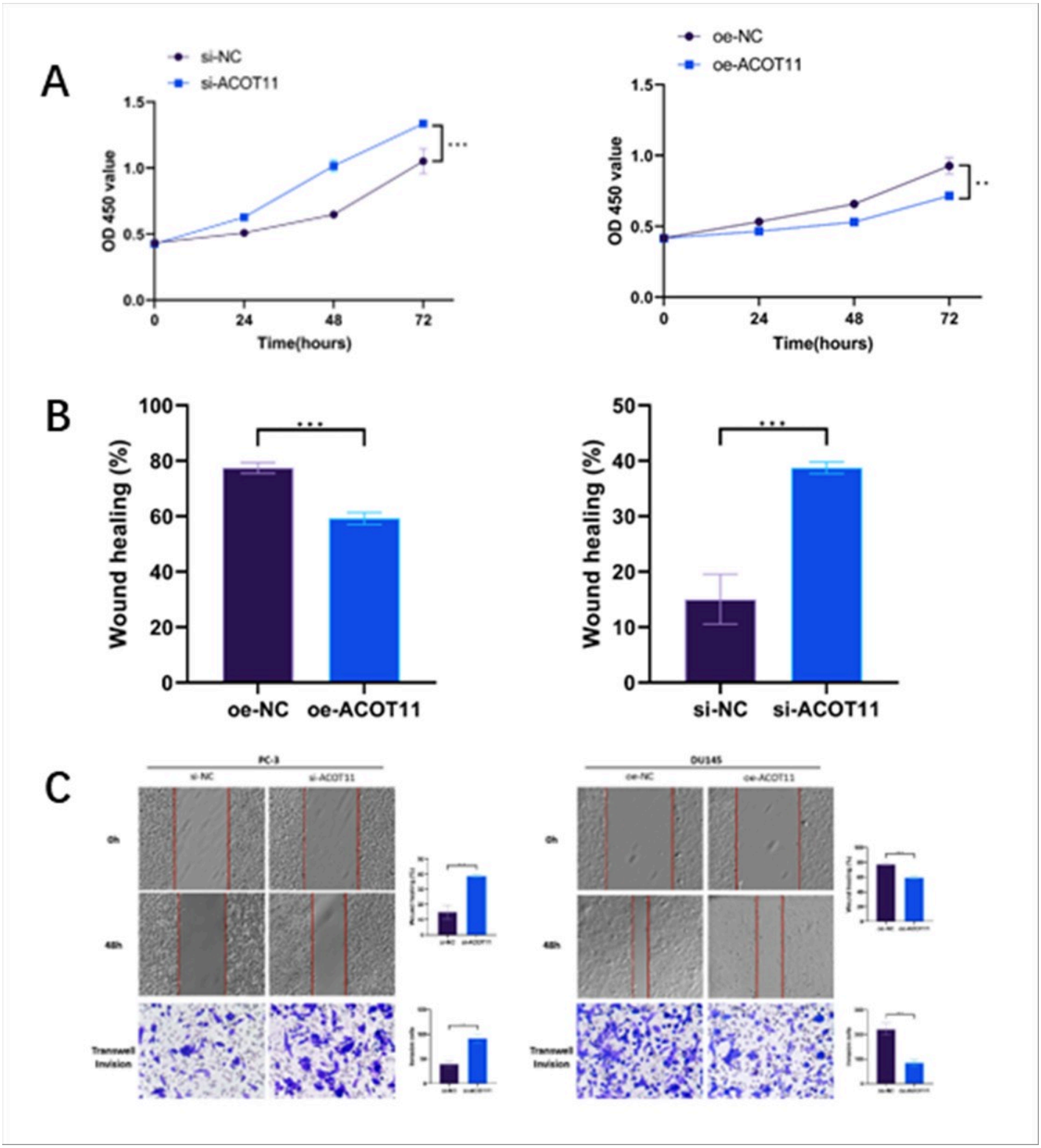


Figure 3

(A)CCK-8 cell proliferation assays in PC-3 and DU145 cells. Cell viability was measured at 0, 24, 48, and 72 hours in si-NC/si-ACOT11 and oe-NC/oe-ACOT11 groups.(B) Quantitative analysis of wound healing assays in PC-3 and DU145 cells. Wound healing rates were compared between si-NC/si-ACOT11 and oe-NC/oe-ACOT11 groups.(C) Wound healing and Transwell invasion assays were performed in PC-3 (si-NC vs si-ACOT11) and DU145 (oe-NC vs oe-ACOT11) cells. Representative images and quantitative analyses are shown.

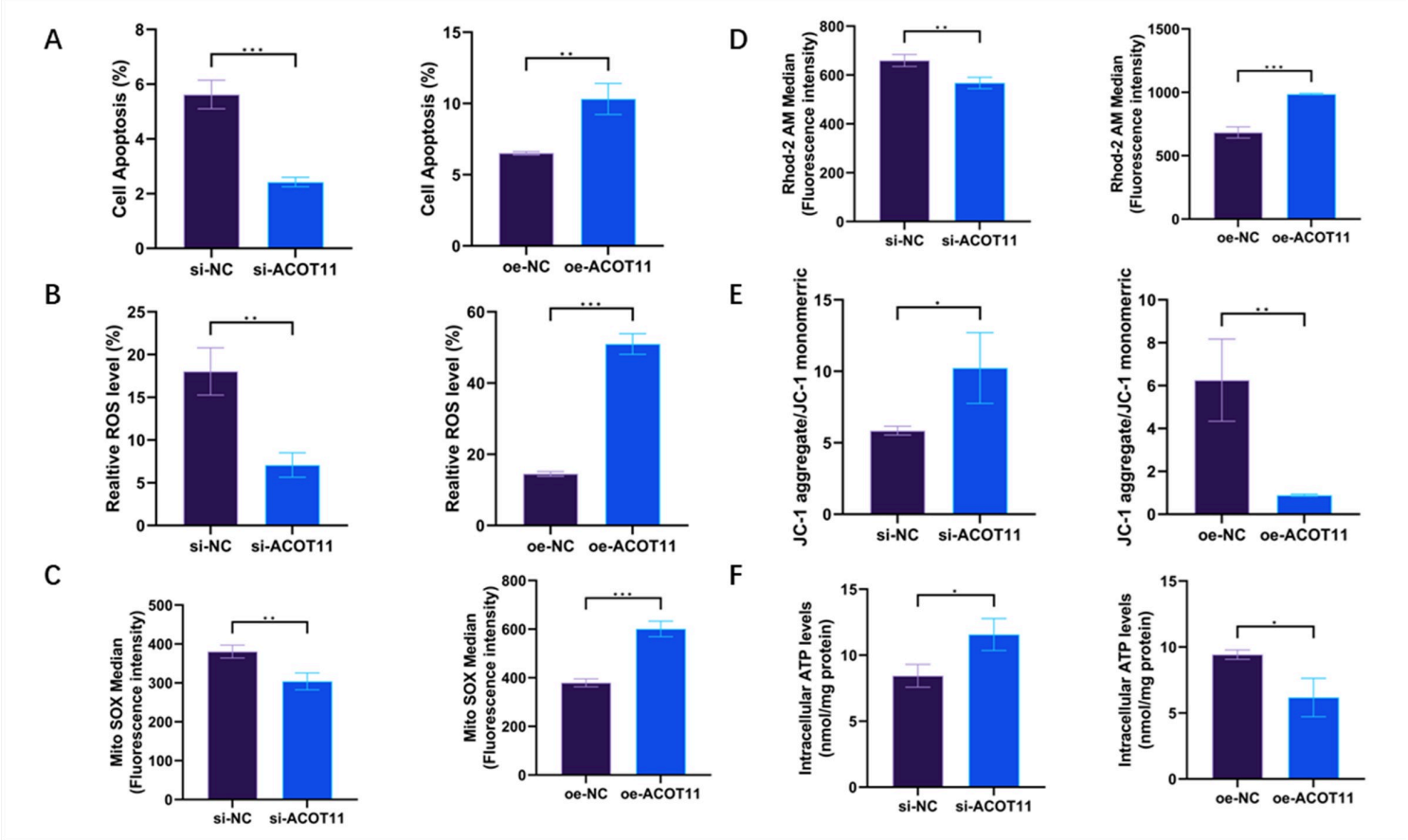


Figure 4

(A)Effects of ACOT11 knockdown and overexpression on cell apoptosis levels in PC-3 cells (si-NC vs si-ACOT11) and DU145 cells (oe-NC vs oe-ACOT11).(B) Effects of ACOT11 knockdown and overexpression on cell ROS levels in PC-3 cells (si-NC vs si-ACOT11) and DU145 cells (oe-NC vs oe-ACOT11).(C)Effects of ACOT11 knockdown and overexpression on mitochondrial ROS and calcium levels in PC-3 (si-NC vs si-ACOT11) and DU145 (oe-NC vs oe-ACOT11) cells.(D) Effects of ACOT11 knockdown and overexpression on calcium (Rhod-2 AM) fluorescence intensities in PC-3 (si-NC vs si-ACOT11) and DU145 (oe-NC vs oe-ACOT11) cells.(E) Effects of ACOT11 knockdown and overexpression on mitochondrial membrane potential (JC-1 aggregate/monomer ratio) in PC-3 (si-NC vs si-ACOT11) and DU145 (oe-NC vs oe-ACOT11) cells.(F)Effects of ACOT11 knockdown and overexpression on intracellular ATP levels in PC-3 (si-NC vs si-ACOT11) and DU145 (oe-NC vs oe-ACOT11) cells.

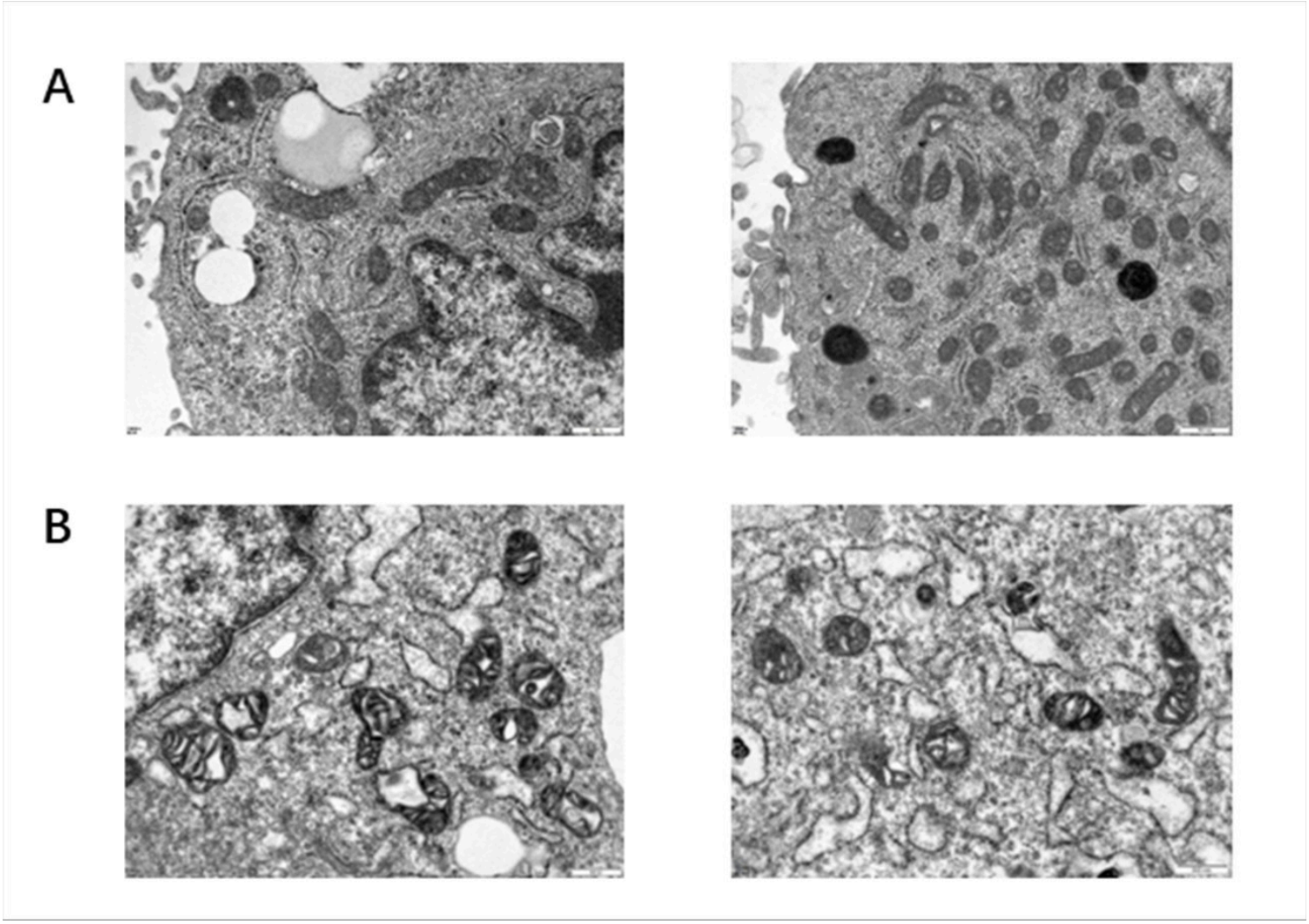


Figure 5

(A) Transmission electron microscopy (TEM) images of mitochondrial ultrastructure in prostate cancer cells. Representative micrographs show mitochondria morphology under si—NC VS si—AOCT-11.(B) High-magnification transmission electron microscopy (TEM) images of mitochondrial ultrastructure in prostate cancer cells. Representative micrographs show detailed mitochondrial morphology under oe--NC oe--ACOT11.

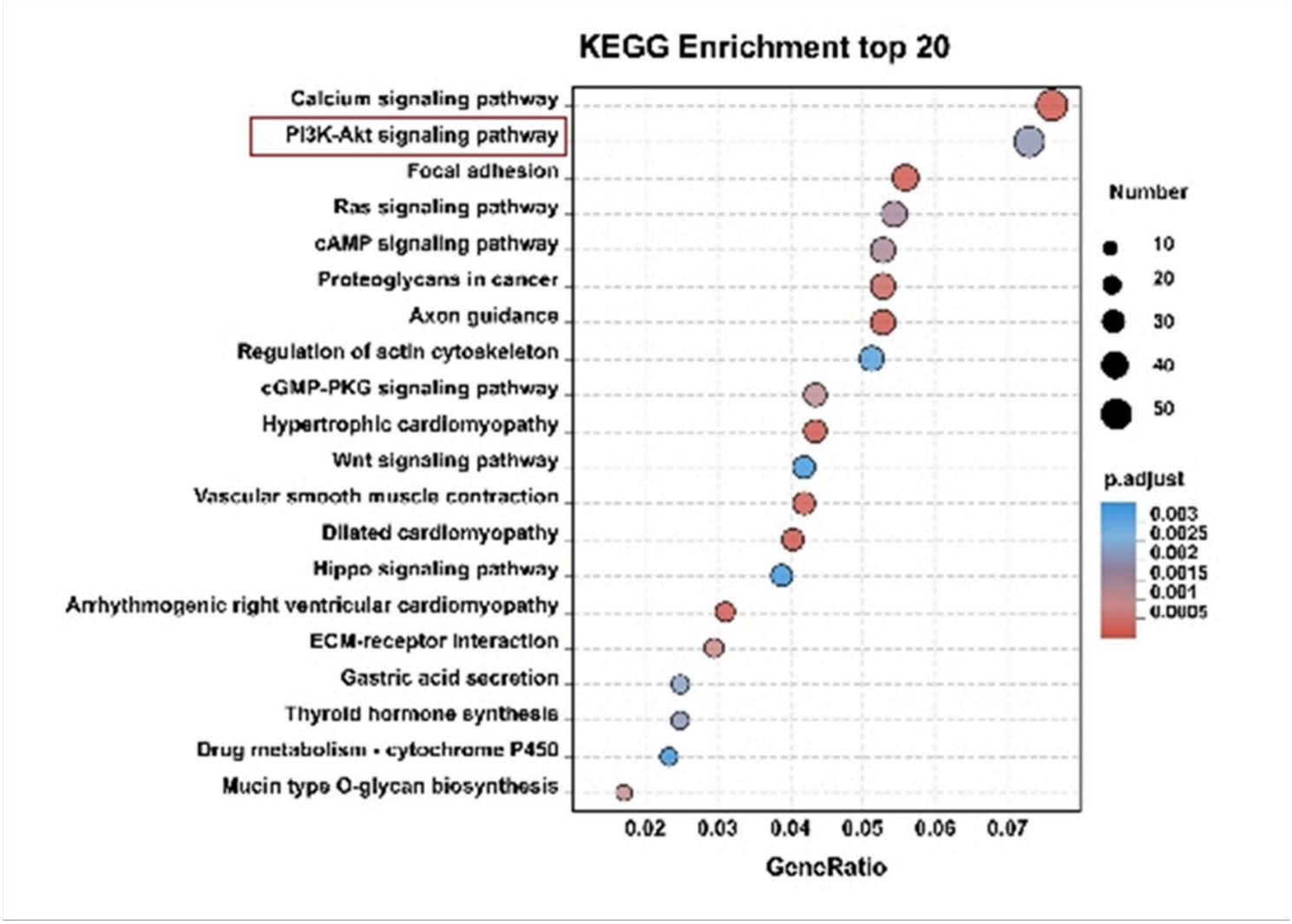


Figure 6

Top 20 enriched KEGG pathways of differentially expressed genes

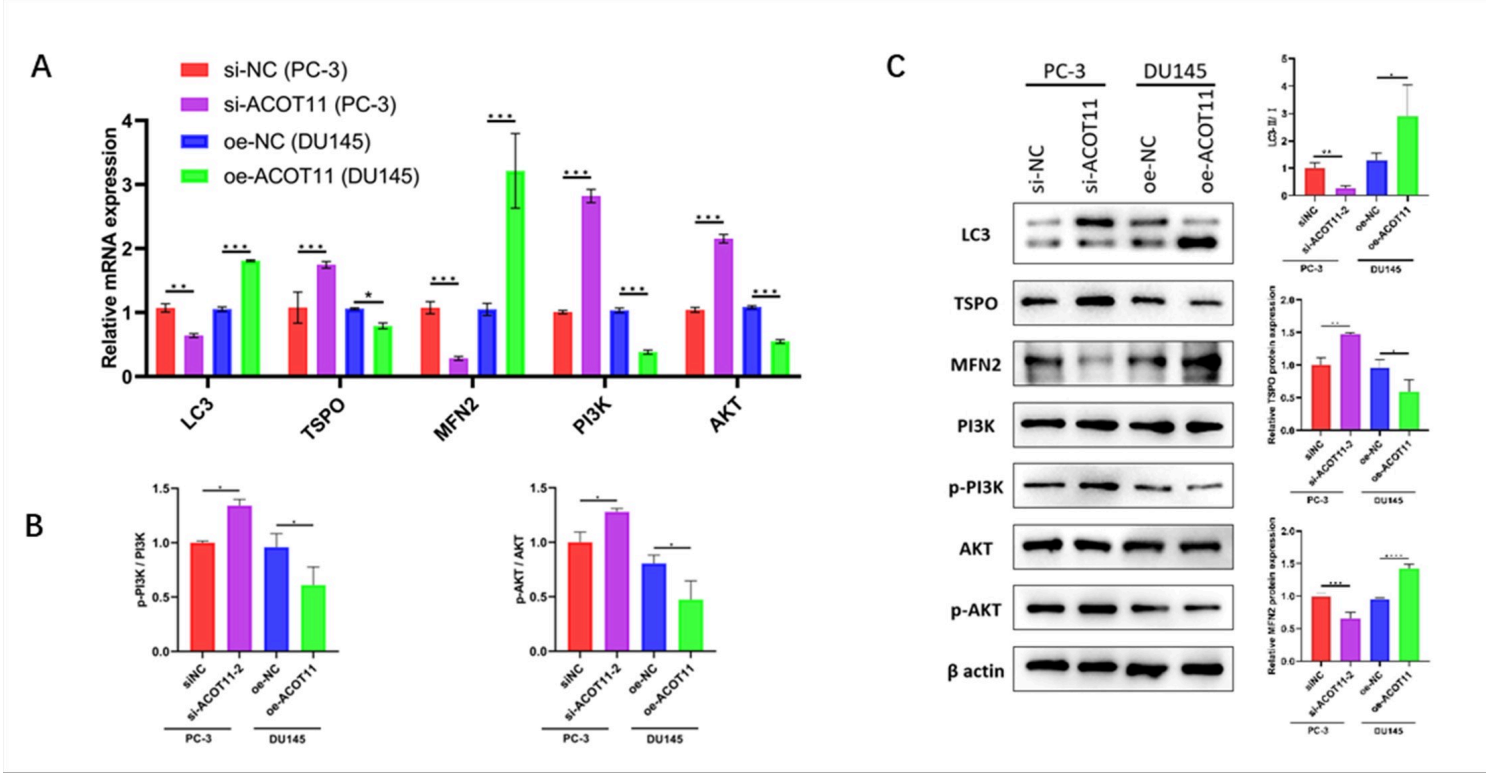


Figure 7

(A) mRNA expression levels of mitochondrial function- and PI3K-Akt pathway-related genes (LC3, TSPO, MFN2, PI3K, AKT) in PC-3 and DU145 cells following ACOT11 knockdown or overexpression.(B) Phosphorylation levels of PI3K and AKT in PC-3 and DU145 cells following ACOT11 knockdown or overexpression. The ratios of p-PI3K/PI3K and p-AKT/AKT are shown.(C).Western blot analysis of autophagy-, mitochondrial function-, and PI3K/AKT pathway-related proteins in PC-3 and DU145 cells following ACOT11 knockdown or overexpression. Quantification of LC3-II/I ratio, TSPO, and MFN2 expression is shown.

Supplementary Files

This is a list of supplementary files associated with this preprint. Click to download.

- TSPO.pdf
- PI3K.pdf
- PPI3K.pdf
- AKT.pdf
- actin.pdf
- LC3.pdf
- MFN2.pdf
- PAKT.pdf

- PC3siACOT11.pdf